Correction of Time-varying PMU Phase Angle Deviation with Unknown Transmission Line Parameters

Ancheng Xue, *Member*, *IEEE*, He Kong, *Student Member*, *IEEE*, Feiyang Xu, *Student Member*, *IEEE*, Junbo Zhao, *Senior Member*, *IEEE*, Naichao Chang, Joe H. Chow, *Life Fellow*, *IEEE*, *Fellow*, *CSEE*, and Haiyan Hong

***Abstract*—Phasor measurement units (PMUs) provide useful data for real-time monitoring of the smart grid. However, there may be time-varying deviation in phase angle differences (PADs) between both ends of the transmission line (TL), which may deteriorate application performance based on PMUs. To address that, this paper proposes two robust methods of correcting time-varying PAD deviation with unknown parameters of TL (ParTL). First, the phenomena of time-varying PAD deviation observed from field PMU data are presented. Two general formulations for PAD estimation are then established. To simplify the formulations, estimation of PADs is converted into the optimal problem with a single ParTL as the variable, yielding a linear estimation of PADs. The latter is used by second-order Taylor series expansion to estimate PADs accurately. To reduce the impact of possible abnormal amplitude data in field data, the IGG (Institute of Geodesy & Geophysics, Chinese Academy of Sciences) weighting function is adopted. Results using both simulated and field data verify the effectiveness and robustness of the proposed methods.**

***Index Terms*—Correction, line parameters, parameter identification, phasor measurement, time-varying phase angle difference deviation.**

I. Introduction

PHASOR measurement units (PMUs) can provide voltage and current phasors for the smart grid [1]. Various applications [2] are developed using data from PMUs, such as early event detection [3], state estimation [4], [5], and parameter estimation [6]. However, due to GPS signal loss [7], GPS spoof attacks [8], [9], manipulation attacks [10], timestamp shift in PMU data [11], power system frequency deviation [12]–[14], etc., the phase angle of PMU data may become less accurate, which could seriously affect their applications. Thus, it is desirable to develop methods that can improve the accuracy of PMUs.

Existing works to improve accuracy of PMU phase angle data can generally be divided into the following three main categories: (1) PMU calibration based on calibrators; (2) PMU algorithm improvement; and (3) PMU data calibration based on a power system model.

Methods in category 1 correct the PMU data based on PMU calibrators [15], [16]. Specifically, the same test signals are sent to both the PMU to be tested and a high precision calibrator. PMU is then calibrated by referring to measured results of the calibrator. These methods are not dependent on power system topology and can directly calibrate a single PMU. However, they can only calibrate PMU offline rather than online and they require additional calibration equipment, which is less economical.

The methods in category 2 improve PMU algorithms [17]–[20] to correct phase angle. In [17], a phasor estimation algorithm is proposed based on the Clarke transform, which can reduce spectrum leakage-caused error. These methods can improve the performance of PMU algorithms effectively. However, they cannot correct errors from current transformer (CT), potential transformer (PT), and PMU device (including analog-to-digital converter, phasor data concentrator, etc.).

Methods in category 3 correct PMU phasors based on the power system models [14], [21]–[30]. These methods do not require additional calibration equipment, and can correct the error caused by a PMU device and transformer online. Specifically, in [21]–[24], PMU data are corrected based on state estimation. For example, in [21], by compensating the phase angle data of PMU at different buses, the location of PMU with deviation and its phase angle deviation are obtained based on state estimation. In [14], [25]–[29], based on the π-type equivalent model of TL and PMU data at both ends of TL, phase angle data are corrected. For example, in [28], a framework for online bias detection and calibration of PMU measurements using density-based spatial clustering of applications is presented, which considers the error in ParTL. In [30], an online calibration method of voltage transformers is presented by adding good quality measurements at optimal

Manuscript received September 27, 2021; revised November 17, 2021; accepted December 31, 2021. Date of online publication August 18, 2022; date of current version September 19, 2022. This work was supported by the National Key Research and Development Program of China (2017YFB0902901) and National Natural Science Foundation of China (51627811).

A. C. Xue (corresponding author, e-mail: acxue@ncepu.edu.cn), H. Kong, F. Y. Xu and H. Y. Hong are with the State Key Laboratory of Alternate Electrical Power System with Renewable Energy Sources, North China Electric Power University, Beijing 102206, China.

J. B. Zhao is with the Department of Electrical and Computer Engineering, University of Connecticut, Storrs, 06268, USA.

N. C. Chang is with National Electric Power Dispatching and Control Center, Beijing 100031, China.

J. H. Chow is with the Department of Electrical, Computer, and Systems Engineering, Rensselaer Polytechnic Institute (RPI), Troy, NY 12180, USA.

DOI: 10.17775/CSEEJPES.2021.07280

locations of the system instead of pre-calibrated PMU.

It is worth noting that, in [21]–[27] and [30], the ParTL are assumed to be known. However, they may change due to weather conditions, and the aging process, resulting in a deviation between the offline value and the true value of ParTL [31]. To deal with this problem, a method to correct the constant PAD deviation independent of ParTL is proposed in [29]. However, by observing field PMU data, the PAD deviation can be time-varying [26]. On the other hand, due to worn-out equipment [32] and communication channel blockage [33], field data are subject to data quality issues [34]. For example, in [34], abnormal data is found in field PMU amplitude data.

To this end, this paper proposes two robust methods of correcting time-varying PAD deviation without knowing ParTL. The main contributions are as follows:

1) Two robust methods for correcting phage angle data with time-varying PADs deviation are proposed without knowing ParTL. The two methods could be both used for ParTL identification when time-varying PAD deviation exists. This differentiates our work as compared to [29], where constant PADs are assumed.

2) The proposed methods have high computational efficiency and are suitable for online applications. In particular, general formulations for the estimation of PADs at multiple snapshots are established. Based on the relationship between PADs and ParTL, high dimensional PAD estimation at multiple snapshots is successfully converted into the optimal problem of low dimensional ParTL estimation. This leads to computation burden reduction.

3) To suppress the influence of abnormal amplitude data caused by channel blockage, worn-out equipment, etc., the IGG method (Institute of Geodesy & Geophysics, Chinese Academy of Sciences) is used to divide data into three categories based on distribution of residual, including normal measurement, available measurement, and harmful measurement. Different categories of data are given different weights to improve the robustness of the proposed method.

The rest of the paper is organized as follows: In Section II, time-varying PAD deviation phenomena are presented. In Section III, based on PMU data at multiple snapshots, two formulations for PAD correction are established. In Section IV, simplification and solution methods for PADs are presented, and adaptive robust estimation of PADs based on IGG method is presented. In Section V and VI, numerical tests and field data results are demonstrated. Finally, conclusions are drawn in Section VII.

II. Time-varying PAD Deviations Observed from Field PMU Data

In this section, the model and power flow equations of TLs are presented first, and then, the time-varying PAD deviation observed from field PMU data is analyzed.

A. Modeling of TLs

High-voltage TLs can be described using the π-type equivalent positive-sequence model, as shown in Fig. 1.

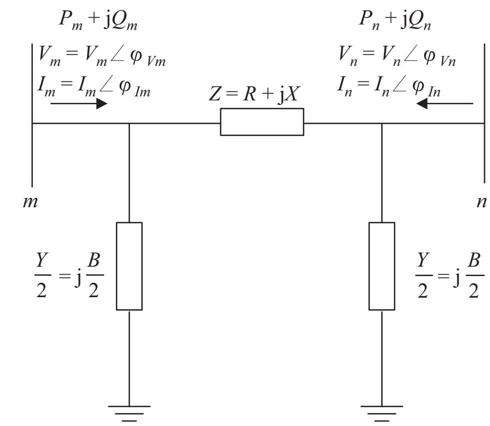

Fig. 1. A π-type equivalent circuit using lumped parameters.

From Fig. 1, active power flows are represented as

$$P_m = gV_m^2 - V_mV_n\cos\theta_V - V_mV_nb\sin\theta_V \tag{1}$$

where $g = R/(R^2+X^2) > 0$, $b = -X/(R^2+X^2) < 0$ and $\theta_V = \arg(\boldsymbol{V}_m/\boldsymbol{V}_n)$, i.e., the true value of PADs.

B. Time-varying Deviation in PADs Observed from Field PMU Data

For a real-world 500 kV, 90.3 km long TL with parameters $R = 1.3781\ \Omega$, $X = 23.8415\ \Omega$, $Y = 4.1280 \times 10^{-4}$ S in China, the field PMU data (data directly obtained from PMUs in realistic power systems) are obtained, including voltage and current phasors, and calculated active and reactive power. Field PADs of PMU across the TL can be directly obtained based on PMU data: see the orange dashed line shown in Fig. 2. Note that since the actual PADs are unknown, PADs from power flow calculations based on offline ParTL are used as reference value instead of actual PADs, see the blue solid line in Fig. 2.

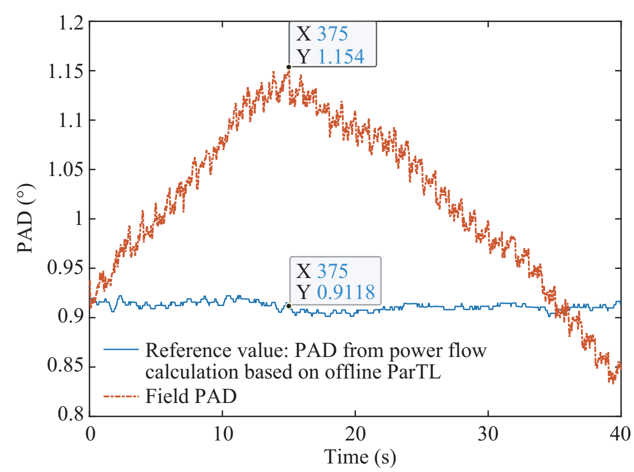

Fig. 2. The estimated and field PADs across both ends of the TL.

In Fig. 2, PADs based on power flow calculation and offline ParTL are constant, i.e., 0.91°, which is consistent with power fluctuations. However, field PADs fluctuate from 0.83° to 1.15°. Thus, there is a time-varying deviation between the field PADs and estimated PADs. This paper aims at correcting the above time-varying PAD deviations without knowing the true value of ParTL.

III. Formulations for PAD Correction Based on Multiple Snapshots of PMU Data

In this section, the relationship between the phase angle data and PADs is first presented. Two estimation models for PADs using two snapshots are then established. Formulations for PADs estimation at multiple snapshots are finally established.

A. Relationship between PADs and Phase Angle Data

To distinguish the true and field electrical quantity, the notation with superscript $'$ is used to denote field PMU data, i.e., $\boldsymbol{V}'_m = V'_m\angle\varphi'_{Vm}$, $\boldsymbol{V}'_n = V'_n\angle\varphi'_{Vn}$, $\boldsymbol{I}'_m = I'_m\angle\varphi'_{Im}$, $\boldsymbol{I}'_n = I'_n\angle\varphi'_{In}$, P'_m, P'_n, Q'_m, Q'_n, while the notation without superscript is used to denote the true value. Besides, let θ'_V denote the field PADs, i.e., $\theta'_V = \angle(\boldsymbol{V}'_m/\boldsymbol{V}'_n)$, and the PAD deviation in field PMU data shown in (2), i.e.,

$$\Delta\theta_V = \theta_V - \theta'_V = (\varphi_{Vm} - \varphi_{Vn}) - (\varphi'_{Vm} - \varphi'_{Vn}) \tag{2}$$

Generally, for one PMU, synchronization between the current and voltage phasors is good locally, thus, the difference between voltage phase angle and current phase angle is accurate, i.e.,

$$\begin{aligned}\varphi_{Vn} - \varphi_{In} &= \varphi'_{Vn} - \varphi'_{In}\\ \varphi_{Vm} - \varphi_{Im} &= \varphi'_{Vm} - \varphi'_{Im}\end{aligned} \tag{3}$$

Furthermore, taking the voltage phase angle data at bus m as a reference, the true value of phase angle data at both ends can be expressed as,

$$\begin{aligned}&\varphi_{Vm} = \varphi'_{Vm} \quad \varphi_{Im} = \varphi'_{Im} \quad \varphi_{Vn} = \varphi'_{Vm} - \theta_V\\ &\varphi_{In} = \varphi_{Vn} - (\varphi_{Vn} - \varphi_{In}) = \varphi'_{Vm} - \theta_V - (\varphi'_{Vn} - \varphi'_{In})\end{aligned} \tag{4}$$

where the phase angle data at both ends of the TL can be represented by PAD. Equation (4) provides a basis for the subsequent establishment of the objective function to reduce the number of variables. Note this paper takes PADs (θ_V) as unknown time-varying variables. It is different from [29] which assumes PAD deviations ($\Delta\theta_V$) as a constant variable.

Since the phase angle is a relative value, any bus could be used as a reference bus. The phase angle of the reference bus is 0 relative to itself. Thus, for PAD estimation across the TL, regardless of whether the phase angle data of the reference bus are calibrated or not, the phase angle data of the reference bus could be regarded as correct.

B. Estimation of PADs using Two Snapshots

In this subsection, two PAD estimation formulations based on the PMU data at two snapshots are established.

1) Model f_{Y} based on Parallel Admittance

According to [35], parallel admittance is expressed as

$$\frac{Y}{2} = \frac{\boldsymbol{I}_m + \boldsymbol{I}_n}{\boldsymbol{V}_m + \boldsymbol{V}_n} \tag{5}$$

Using the PMU data under two different power flows, the current and voltage phasors at both ends of the TL hold, i.e.,

$$\frac{\boldsymbol{I}_{m1} + \boldsymbol{I}_{n1}}{\boldsymbol{V}_{m1} + \boldsymbol{V}_{n1}} = \frac{\boldsymbol{I}_{m2} + \boldsymbol{I}_{n2}}{\boldsymbol{V}_{m2} + \boldsymbol{V}_{n2}} = \frac{Y}{2} \tag{6}$$

where $\boldsymbol{I}_{m1}$, $\boldsymbol{I}_{m2}$, $\boldsymbol{V}_{m1}$, $\boldsymbol{V}_{m2}$, $\boldsymbol{I}_{n1}$, $\boldsymbol{I}_{n2}$, $\boldsymbol{V}_{n1}$, $\boldsymbol{V}_{n2}$ denote the true values of phasors under power flows 1 and 2. (6) can be further rewritten as

$$\begin{aligned}f_{\mathrm{Y}}^{*} &= (\boldsymbol{I}_{m1} + \boldsymbol{I}_{n1})(\boldsymbol{V}_{m2} + \boldsymbol{V}_{n2}) - (\boldsymbol{I}_{m2} + \boldsymbol{I}_{n2})(\boldsymbol{V}_{m1} + \boldsymbol{V}_{n1})\\ &= 0\end{aligned} \tag{7}$$

With the field PMU voltage and current phasor amplitudes and (4), (7) can be rewritten as (8).

$$\begin{aligned}&f_{\mathrm{Y}}^{*}(\theta_{V1}, \theta_{V2}) =\\ &\quad (I'_{m1}\angle\varphi'_{Im1} + I'_{n1}\angle(\varphi'_{Vm1} - \theta_{V1} - (\varphi'_{Vn1}\\ &\quad - \varphi'_{In1}(V'_{m2}\angle\varphi'_{Vm2} + V'_{n2}\angle(\varphi'_{Vm2} - \theta_{V2}))\\ &\quad - (I'_{m2}\angle\varphi'_{Im2} + I'_{n2}\angle(\varphi'_{Vm2} - \theta_{V2} - (\varphi'_{Vn2}\\ &\quad - \varphi'_{In2}(V'_{m1}\angle\varphi'_{Vm1} + V'_{n1}\angle(\varphi'_{Vm1} - \theta_{V1})) = 0\end{aligned} \tag{8}$$

In (8), θ_{V1} and θ_{V2} respectively denote true PADs to be solved under power flows 1 and 2. (8) has unknown variables θ_{V1} and θ_{V2}, and must be solved using the PMU data under different power flow conditions.

Due to voltage and current scaling and quantization error, the field data contains measurement noise. Thus, even if θ_{V1} and θ_{V2} are the true value of PADs, $f_{\mathrm{Y}}^{*}(\theta_{V1}, \theta_{V2})$ is not exactly zero, i.e.,

$$f_{\mathrm{Y}}(\theta_{V1}, \theta_{V2}) = \varepsilon_{\mathrm{Y}} \tag{9}$$

where ε_{Y} is the residual error of f_{Y}. Thus, solving (9) directly will be affected by noise. Instead, the PADs can be obtained by solving the following minimization problem:

$$\min |f_{\mathrm{Y}}(\theta_{V1}, \theta_{V2})|, \theta_{V1}, \theta_{V2} \in (-\pi, \pi] \tag{10}$$

where $|\cdot|$ represents the module of complex number.

2) Model f_{Z} based on Series Impedance

According to [35], the equivalent impedance of the TL can also be expressed as

$$Z = \frac{\boldsymbol{V}_m^2 - \boldsymbol{V}_n^2}{\boldsymbol{I}_m\boldsymbol{V}_n - \boldsymbol{I}_n\boldsymbol{V}_m} \tag{11}$$

Similar to Section III-B. 2), the current and voltage phasors under two power flows satisfy

$$\frac{\boldsymbol{V}_{m1}^2 - \boldsymbol{V}_{n1}^2}{\boldsymbol{I}_{m1}\boldsymbol{V}_{n1} - \boldsymbol{I}_{n1}\boldsymbol{V}_{m1}} = \frac{\boldsymbol{V}_{m2}^2 - \boldsymbol{V}_{n2}^2}{\boldsymbol{I}_{m2}\boldsymbol{V}_{n2} - \boldsymbol{I}_{n2}\boldsymbol{V}_{m2}} = Z \tag{12}$$

Furthermore, (12) can be rewritten as

$$\begin{aligned}f_{\mathrm{Z}}^{*} &= (\boldsymbol{V}_{m2}^2 - \boldsymbol{V}_{n2}^2)(\boldsymbol{I}_{m1}\boldsymbol{V}_{n1} - \boldsymbol{I}_{n1}\boldsymbol{V}_{m1})\\ &\quad - (\boldsymbol{V}_{m1}^2 - \boldsymbol{V}_{n1}^2)(\boldsymbol{I}_{m2}\boldsymbol{V}_{n2} - \boldsymbol{I}_{n2}\boldsymbol{V}_{m2}) = 0\end{aligned} \tag{13}$$

Similar to (8), based on the field PMU voltage and current measurements, (13) can be rewritten as an equation with the true value of PADs as variables, see (14).

$$\begin{aligned}&f_{\mathrm{Z}}^{*}(\theta_{V1}, \theta_{V2}) =\\ &\quad ((V'_{m2}\angle\varphi'_{Vm2})^2 - (V'_{n2}\angle(\varphi'_{Vm2} - \theta_{V2}))^2)\end{aligned}$$

$$\begin{aligned}&(I'_{m1}V'_{n1}\angle(\varphi'_{Im1}+(\varphi'_{Vm1}-\theta_{V1}))-I'_{n1}V'_{m1}\angle((\varphi'_{Vm1}\\&-\theta_{V1}-(\varphi'_{Vn1}-\varphi'_{In1}))+\varphi'_{Vm1})-((V'_{m1}\angle\varphi'_{Vm2})^2\\&-(V'_{n1}\angle(\varphi'_{Vm1}-\theta_{V1}))^2)(I'_{m2}V'_{n2}\angle(\varphi'_{Im2}\\&+(\varphi'_{Vm2}-\theta_{V2}))-I'_{n2}V'_{m2}\angle((\varphi'_{Vm2}-\theta_{V2}\\&-(\varphi'_{Vn2}-\varphi'_{In2}))+\varphi'_{Vm2}))=0\end{aligned} \tag{14}$$

If measurement noise is considered, (14) becomes

$$f_{\mathrm{Z}}(\theta_{V1},\theta_{V2})=\varepsilon_{\mathrm{Z}} \tag{15}$$

where ε_{Z} is the residual error of f_{Z}. Similarly, PADs can also be obtained by solving the following minimization problem (16):

$$\min\left|f_{\mathrm{Z}}(\theta_{V1},\theta_{V2})\right|,\theta_{V1},\theta_{V2}\in(-\pi,\pi] \tag{16}$$

As (10) and (16) are objective functions with similar forms, they can be written uniformly as

$$\min\left|f(\theta_{V1},\theta_{V2})\right|,\theta_{V1},\theta_{V2}\in(-\pi,\pi] \tag{17}$$

where f includes f_{Z} and f_{Y}. Furthermore, it is necessary to extend (17) to estimate the PADs at multiple snapshots.

C. Estimation of PADs using Multiple Snapshots

The PMU data under two different power flows with $2n$ snapshots are needed to expand (17). Let $\boldsymbol{M}'_i=[V'_{m,i}, \varphi'_{Vm,i}, V'_{n,i}, \varphi'_{Vn,i}, I'_{m,i}, \varphi'_{Im,i}, I'_{n,i}, \varphi'_{In,i}, P'_{m,i}, P'_{n,i}, Q'_{m,i}, Q'_{n,i}]$ represent field PMU measurement vectors at snapshots i. $\boldsymbol{M}'_{1,i}$ and $\boldsymbol{M}'_{2,i}$ denote the measurement vectors at snapshot i under power flows 1 and 2. The data combination method is shown in Fig. 3.

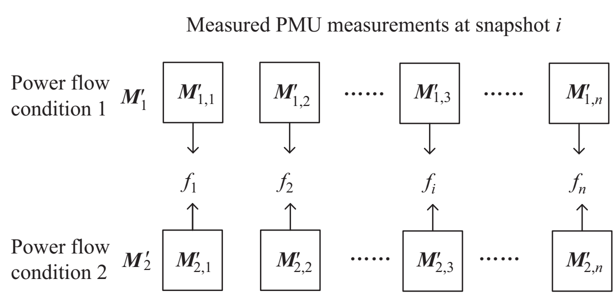

Fig. 3. The data combination method.

Based on the above data combination method, (17) is extended as

$$\begin{aligned}&\min F(\theta_{V1,1},\theta_{V2,1},\cdots,\theta_{V1,n},\theta_{V2,n})\\&=\min\sum_{i=1}^{n}\left|f_i(\boldsymbol{M}'_{1,i},\boldsymbol{M}'_{2,i},\theta_{V1,i},\theta_{V2,i})\right|\end{aligned} \tag{18}$$

where $\boldsymbol{M}'_{1,i}$ and $\boldsymbol{M}'_{2,i}$ are the known PMU measurements, while $\theta_{V1,i},\theta_{V2,i}$ are the unknown variables to be solved. When solving (18), some attention needs to be paid to:

1) For each f_i, two variables are solved based on two PMU snapshots, which means the equation has low measurement redundancy. Thus, estimation results ($\theta_{V,i}$) are highly susceptible to measurement noise.

2) There are $2n$ variables in (18), which require extensive computations. It needs to be simplified for computational efficiency improvement without loss of accuracy.

IV. Proposed Estimation Methods for PADs

A. Proposed Solution Framework

The framework of the proposed methods is shown in Fig. 4 and it contains linear estimation for PADs, rough identification for ParTL, and accurate estimation for PADs. Detailed steps for the proposed methods are in Fig. 4.

Step 1: Linear estimation of PADs

In this step, the approximated relationship between PADs ($\Delta\theta_{V,i}$) and reactance (X) is derived first. With that relationship, a simplified formulation to estimate reactance is obtained. Furthermore, with the result of estimated reactance, linear estimation for the PADs can be obtained with the above relationship.

Step 2: Rough identification for ParTL

In this step, first, the phase angle data at both ends of the TL are estimated with Eq. (4) and the linearly estimated PADs. Then, the ParTL is identified roughly.

Step 3: Accurate estimation for PADs

In this step, the approximated relationship between the PADs and series conductance (g) and admittance (b) is derived first, with the second order Taylor expansion at the linear estimation of PADs.

With the above relationship, the simplified formulation to estimate the series conductance (g) and admittance (b) is obtained.

Furthermore, with the results of estimated series conductance and admittance, PADs can be obtained accurately with the above relationship.

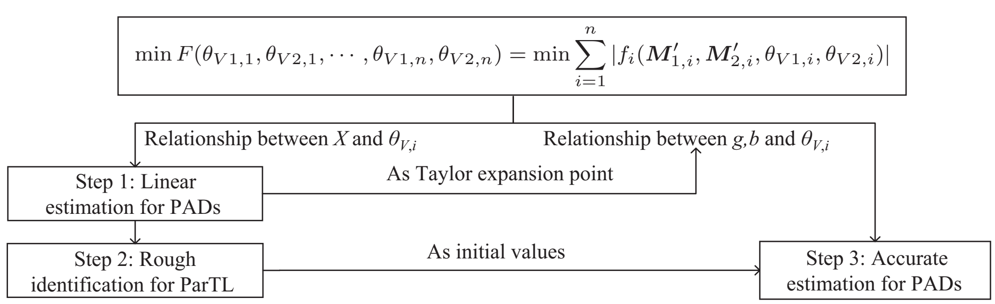

Fig. 4. The framework for simplification and solution of the formulation for PADs.

B. Linear Estimation for PADs with Multiple PMU Snapshots

1) Approximated Relationship Between PADs and Reactance

For high-voltage TL, $R \ll X$, that is, $b \gg g$, and $b \approx -1/X$, $g \approx 0$. In most cases, θ_V is generally small (e.g., less than 7°) so that $\sin\theta_V \approx \theta_V$ and $\cos\theta_V \approx 1$. Thus, (1) can be simplified as

$$P_{m,i} \approx -V_{m,i}V_{n,i}b\sin\theta_{V,i} \approx V_{m,i}V_{n,i}\theta_{V,i}/X \tag{19}$$

Thus, the PADs ($\theta_{V,i}$) can be estimated using

$$\theta_{V,i} \approx \frac{P_{m,i}X}{V_{m,i}V_{n,i}} \tag{20}$$

Equation (20) is the approximated relationship between PADs and reactance

2) Formulation of Linear Estimation for PADs

Combining (20) and (18), the linear formulation for PADs at multiple snapshots can be established as

$$\begin{cases} \min \sum_{i=1}^{n} \left| f_i(\boldsymbol{M}'_{1,i}, \boldsymbol{M}'_{2,i}, \theta_{V1,i}, \theta_{V2,i}) \right| \\ \theta_{V1,i} \approx P'_{m1,i}X/V'_{m1,i}V'_{n1,i} \\ \theta_{V2,i} \approx P'_{m2,i}X/V'_{m2,i}V'_{n2,i} \end{cases} \tag{21}$$

$$\begin{aligned} &\Rightarrow \min \sum_{i=1}^{n} \left| f_i\left(\boldsymbol{M}'_{1,i}, \boldsymbol{M}'_{2,i}, \frac{P'_{m1,i}X}{V'_{m1,i}V'_{n1,i}}, \frac{P'_{m2,i}X}{V'_{m2,i}V'_{n2,i}}\right) \right| \\ &= \min \sum_{i=1}^{n} \left| f_i^{\mathrm{L}}(\boldsymbol{M}'_{1,i}, \boldsymbol{M}'_{2,i}, X) \right| = \min F^{\mathrm{L}}(X) \\ &= \min \sum_{i=1}^{n} \left| \varepsilon_i^{\mathrm{L}} \right| \end{aligned} \tag{22}$$

where $f_i^{\mathrm{L}}(\boldsymbol{M}'_{1,i}, \boldsymbol{M}'_{2,i}, X)$ represents a new function obtained by replacing $\theta_{V1,i}, \theta_{V2,i}$ in $f_i(\boldsymbol{M}'_{1,i}, \boldsymbol{M}'_{2,i}, \theta_{V1,i}, \theta_{V2,i})$ using (20), and $\varepsilon_i^{\mathrm{L}}$ is the residual including $\varepsilon_{\mathrm{Y},i}^{\mathrm{L}}$ and $\varepsilon_{\mathrm{Z},i}^{\mathrm{L}}$.

Equation (22) can be solved by dichotomy, and the optimal solution of (22) is donated as $X_{\mathrm{op}}^{\mathrm{L}}$. Once $X_{\mathrm{op}}^{\mathrm{L}}$ is obtained, then, the PADs at different snapshots which are denoted as $\theta_{V1,1}^{0}$, $\theta_{V2,1}^{0}, \cdots, \theta_{V1,n}^{0}, \theta_{V2,n}^{0}$, can be calculated linearly with (20). The overall solution process is as follows.

$$\begin{array}{l} \min F^{\mathrm{L}}(X) \xrightarrow{\text{dichotomy}} X_{\mathrm{op}}^{\mathrm{L}} \xrightarrow{\theta_{V,i}^{0} \approx \frac{P'_{m,i}}{V'_{m,i}V'_{n,i}} X_{\mathrm{op}}^{\mathrm{L}}} \theta_{V1,i}^{0}, \theta_{V2,i}^{0} \\ \quad i = 1, 2, \ldots, n \end{array}$$

Fig. 5. Flow chart of the linear estimation of PADs.

Besides, about the boundary of dichotomy, according to [36], the maximal deviation of offline reactance value is ±10%. Thus, to cover the true value of reactance effectively, the search boundary of dichotomy is set to be $[0.6X_{\text{offline}}, 1.4X_{\text{offline}}]$, and the convergence criterion is $|X^k - X^{k+1}| < 0.001X_{\text{offline}}$.

Based on linear simplification, (18) is converted into (22). Note, in (18), $2n$ variables are solved based on PMU data at $2n$ snapshots, but, in (22), one variable is solved based on PMU data at $2n$ snapshots. Therefore, redundancy is higher, yielding better robustness to measurement noise.

C. Rough Identification of ParTL

Once the estimation results of PADs using linear approximations are obtained, the phase angles at both ends of the TL can be roughly corrected based on (4). The corresponding corrected phasors are denoted as $\boldsymbol{V}'_{m\mathrm{RC},i}$, $\boldsymbol{V}'_{n\mathrm{RC},i}$, $\boldsymbol{I}'_{m\mathrm{RC},i}$, $\boldsymbol{I}'_{n\mathrm{RC},i}$ at snapshot i. Furthermore, using the corrected data at snapshot i, the ParTL can be identified as

$$X_i = \mathrm{imag}\left(\frac{\boldsymbol{V}'^2_{m\mathrm{RC},i} - \boldsymbol{V}'^2_{n\mathrm{RC},i}}{\boldsymbol{I}'_{m\mathrm{RC},i}\boldsymbol{V}'_{n\mathrm{RC},i} - \boldsymbol{I}'_{n\mathrm{RC},i}\boldsymbol{V}'_{m\mathrm{RC},i}}\right) \tag{23}$$

$$R'_i = \mathrm{real}\left(\frac{\boldsymbol{V}'^2_{m\mathrm{RC},i} - \boldsymbol{V}'^2_{n\mathrm{RC},i}}{\boldsymbol{I}'_{m\mathrm{RC},i}\boldsymbol{V}'_{n\mathrm{RC},i} - \boldsymbol{I}'_{n\mathrm{RC},i}\boldsymbol{V}'_{m\mathrm{RC},i}}\right) \tag{24}$$

where X_i, R'_i represent rough identification results of ParTL at snapshot i.

Furthermore, considering that resistance is hard to identify, as the sensitivity of resistance to voltage amplitude may be very high [35], small deviations in filed voltage amplitude will result in large deviations in resistance. For example, to a TL with $X/R = 14$, and $\Delta\theta_V = 0.8°$ (0.014 rad), the sensitivity is -1000 [35], which means that 0.1% error in voltage will result in 100% error in resistance.

To address this problem, considering the ratio between reactance and resistance changes little, resistance can also be identified based on identification results of reactance, i.e.,

$$R''_i = \frac{X_i}{K_{\mathrm{X/R}}} \tag{25}$$

where $K_{\mathrm{X/R}} = X_{\text{offline}}/R_{\text{offline}}$, X_{offline} and R_{offline} are the offline values of reactance and resistance, and R'' is the identified resistance based on the ratio between reactance and resistance.

On the other hand, when the accuracy of voltage amplitude is high, the identified results based on (24) are more accurate; when the accuracy of voltage amplitude is low, the identified results based on (25) is more accurate. Since R'_i is more sensitive to the accuracy of voltage, deviation between R'_i and R_{offline} can be used as a criterion for selection, i.e.,

$$R_i \begin{cases} R'_i & R'_i - R_{\text{offline}} < \alpha R_{\text{offline}} \\ R''_i & R'_i - R_{\text{offline}} > \alpha R_{\text{offline}} \end{cases} \tag{26}$$

Generally, the change of resistance does not exceed 30% [37], thus, α is set to be 30% in this paper.

Furthermore, based on identified results at multiple snapshots, i.e., $\boldsymbol{R} = [R_1, R_2, \cdots, R_{2n}]$, $\boldsymbol{X} = [X_1, X_2, \cdots, X_{2n}]$, rough estimation for the ParTL can be obtained with the median estimation [38].

$$R_0 = \mathrm{Median}(\boldsymbol{R}) \quad X_0 = \mathrm{Median}(\boldsymbol{X}) \tag{27}$$

The rough estimation results of ParTL are denoted as $Z_0 = R_0 + \mathrm{j}X_0 = 1/(g_0 + \mathrm{j}b_0)$, which will be used as initial values for accurate estimation of PADs.

D. Accurate Estimation of PADs

1) Approximated Relationship Between PADs and Series Conductance and Admittance

Since resistance is ignored and $\sin\theta_V \approx \theta_V$ and $\cos\theta_V \approx 1$ in (20), the linear approximation of PADs in Section IV-B contains errors. To improve accuracy, estimated results of PADs ($\theta^0_{V,i}$) are taken as the Taylor expansion point, the second-order Taylor series expansion of $\cos\theta_{V,i}$ and $\sin\theta_{V,i}$ in (1) can be obtained as follows:

$$\sin\theta_{V,i} \approx A_{\mathrm{s},i}\theta^2_{V,i} + B_{\mathrm{s},i}\theta_{V,i} + C_{\mathrm{s},i} \tag{28}$$

$$\cos\theta_{V,i} \approx A_{\mathrm{c},i}\theta^2_{V,i} + B_{\mathrm{c},i}\theta_{V,i} + C_{\mathrm{c},i} \tag{29}$$

where

$$\begin{aligned}
&A_{\mathrm{s},i} = -\sin\left(\theta^0_{V,i}\right)/2,\ B_{\mathrm{s},i} = \cos\theta^0_{V,i} + \theta^0_{V,i}\sin\theta^0_{V,i},\\
&C_{\mathrm{s},i} = \sin\theta^0_{V,i} - \theta^0_{V,i}\cos\theta^0_{V,i} - \left(\theta^0_{V,i}\right)^2\sin\left(\theta^0_{V,i}\right)/2\\
&A_{\mathrm{c},i} = -\cos\left(\theta^0_{V,i}\right)/2,\ B_{\mathrm{c},i} = -\sin\theta^0_{V,i} + \theta^0_{V,i}\cos\theta^0_{V,i},\\
&C_{\mathrm{c},i} = \cos\theta^0_{V,i} + \theta^0_{V,i}\sin\theta^0_{V,i} - \frac{1}{2}\left(\theta^0_{V,i}\right)^2\cos\theta^0_{V,i}
\end{aligned}$$

With (28)–(29) and the field PMU voltage and current phasor data at snapshot i, (1) can be rewritten as

$$\begin{aligned}
P'_{m,i} \approx\ & (V'^2_{m,i} - V'_{m,i}V'_{n,i}(A_{\mathrm{c},i}\theta^2_{V,i} + B_{\mathrm{c},i}\theta_{V,i} + C_{\mathrm{c},i}))g\\
& - V'_m V'_n(A_{\mathrm{s},i}\theta^2_{V,i} + B_{\mathrm{s},i}\theta_{V,i} + C_{\mathrm{s},i})b
\end{aligned} \tag{30}$$

Equation (30) is a quadratic equation for $\theta_{V,i}$ and the following estimation can be obtained:

$$\theta_{V,i} = \frac{-B_i(g,b) + \sqrt{B^2_i(g,b) - 4A_i(g,b)C_i(g,b)}}{2A_i(g,b)} \tag{31}$$

where $A_i = -V'_{m,i}V'_{n,i}A_{\mathrm{c},i}g - V'_{m,i}V'_{n,i}A_{\mathrm{s},i}b$, $B_i = -V'_{m,i}V'_{n,i}B_{\mathrm{c},i}g - V'_{m,i}V'_{n,i}B_{\mathrm{s},i}b$, $C_i = V'^2_{m,i}g - V'_{m,i}V'_{n,i}C_{\mathrm{c}}g - V'_{m,i}V'_{n,i}C_{\mathrm{s},i}b - P'_{m,i}$.

Equation (31) is the approximated relationship between PADs and series conductance and admittance, where $\theta^0_{V,i}$, $P'_{m,i}$, $V'_{m,i}$, $V'_{n,i}$ are known variables; $\theta_{V,i}$ and g,b are unknown variables, Thus, once the g,b is obtained, the PADs can be obtained.

During system operations, typically $\theta_{V,i} < 7^\circ$ (0.12 rad) and $g \approx 0$, $b \approx -1/X$, $V_{m,i}V_{n,i} > 10^4$, thus, $-B_i$ is far larger than π; By contrast, as $A_{\mathrm{c},i} \approx -0.5, g \approx 0, A_{s,i} \approx 0$, A_i is small. Therefore, the other root, i.e., $\theta_{V,i} = (-B_i - \sqrt{B^2_i - 4A_iC_i})/2A_i \gg \pi$, which should be discarded.

2) Formulation for Accurate Estimation of PADs

Combining (31) and (18), an accurate formulation for PADs at multiple snapshots can be established as

$$\begin{cases}
\min\sum_{i=1}^n\left|f_i\left(\boldsymbol{M}'_{1,i},\boldsymbol{M}'_{2,i},\theta_{V1,i},\theta_{V2,i}\right)\right|\\
\theta_{V1,i} = \frac{-B_{1,i}+\sqrt{B^2_{1,i}-4A_{1,i}C_{1,i}}}{2A_{1,i}}\\
\theta_{V2,i} = \frac{-B_{2,i}+\sqrt{B^2_{2,i}-4A_{2,i}C_{2,i}}}{2A_{2,i}}
\end{cases} \tag{32}$$

$$\begin{aligned}
\Rightarrow \min\sum_{i=1}^n\Bigg|f_i\Bigg(&\boldsymbol{M}'_{1,i},\boldsymbol{M}'_{2,i},\frac{-B_{1,i}+\sqrt{B^2_{1,i}-4A_{1,i}C_{1,i}}}{2A_{1,i}},\\
&\frac{-B_{2,i}+\sqrt{B^2_{2,i}-4A_{2,i}C_{2,i}}}{2A_{2,i}}\Bigg)\Bigg|\\
= \min\sum_{i=1}^n&\left|f^{\mathrm{A}}_i\left(\boldsymbol{M}'_{1,i},\boldsymbol{M}'_{2,i},g,b\right)\right| = \min F^{\mathrm{A}}(g,b)
\end{aligned} \tag{33}$$

where $A_{1,i}$ and $A_{2,i}$ are the functions of g,b, which are obtained by bringing the PMU data under power flow 1 and power flow 2 into $A_i(g,b)$ respectively. This also applied to $B_{1,i}$ $B_{2,i}$ $C_{1,i}$ $C_{2,i}$.

Furthermore, (33) can be solved using the interior point method (IPM). Optimal solutions to $\min F^{\mathrm{A}}(g,b)$ are denoted as $g^{\mathrm{A}}_{\mathrm{op}}$ and $b^{\mathrm{A}}_{\mathrm{op}}$. Once $g^{\mathrm{A}}_{\mathrm{op}}$ and $b^{\mathrm{A}}_{\mathrm{op}}$ are obtained, using (31), the PADs at different snapshots can be estimated accurately. The flow chart is shown in Fig. 6.

$$\begin{aligned}
&\min F^{\mathrm{A}}(g,b) \xrightarrow{\mathrm{IPM}} g^{\mathrm{A}}_{\mathrm{op}} \text{ and } b^{\mathrm{A}}_{\mathrm{op}}\\
&\qquad\xrightarrow{\theta_{V,i}\approx\frac{-B_i+\sqrt{B^2_i-4A_iC_i}}{2A_i}} \theta_{V1,i} \text{ and } \theta_{V2,i}\\
&\qquad i = 1,2,\ldots,n
\end{aligned}$$

Fig. 6. The flow chart for accurate estimation of PADs.

Considering the interior point method is dependent on good initial conditions, the rough identification results of ParTL in Section IV-C (i.e., g_0 and b_0) are used for the initial value. Since the rough identification based on dichotomy has good astringency and the results are close to true value, it can provide good initial values to ensure accuracy of the proposed methods. Besides, after a large number of simulations, the search boundary is set as $[0.6g_0, 1.4g_0]$, $[1.3b_0, 0.7b_0]$.

Based on (33), the estimation of PADs at multiple snapshots is converted to the optimal problem for g,b, i.e., estimate g,b to minimize $F^{\mathrm{A}}(g,b)$. This helps reduce the number of variables and improves measurement redundancy.

3) Robust Estimation of PADs

To resist the influence of possible bad PMU amplitude data issues (including bad data of voltage and current amplitude, active and reactive power), development of robust estimation of PADs is advocated. In particular, the objective functions (22) and (33) are changed to the following weighted objective function,

$$\min F^{\mathrm{LW}}(X) = \min\sum_{i=1}^n w_i\left|f^{\mathrm{L}}_i\left(\boldsymbol{M}'_{1,i},\boldsymbol{M}'_{2,i},X\right)\right| \tag{34}$$

$$\min F^{\mathrm{AW}}(g,b) = \min\sum_{i=1}^n w_i\left|f^{\mathrm{A}}_i\left(\boldsymbol{M}'_{1,i},\boldsymbol{M}'_{2,i},g,b\right)\right| \tag{35}$$

where F^{LW} and F^{AW} respectively represent weighted linear and accurate objective functions of PADs based on (22) and (33). With different weights at different snapshots, the influence of abnormal data can be reduced. For example, when abnormal data occur, the corresponding weight in the objective function can be set to 0, and the measurement is rejected.

This paper applies the IGG (Institute of Geodesy & Geophysics) method shown in [39], [40] to determine measurement weights. The IGG method divides measurement data into three categories: 1) normal measurement; 2) available measurement; 3) harmful measurement. Correspondingly, weight is divided into three categories: 1) security zone; 2) weight down zone; 3) elimination zone. The weight function of IGG is

$$w_i(\varepsilon_i^{\mathrm{L}}) = \begin{cases} 1 & |\varepsilon_i^{\mathrm{L}} - \mu| \le s\sigma_0 \\ \frac{s\sigma_0}{|\varepsilon_i^{\mathrm{L}} - \mu|} & s\sigma_0 < |\varepsilon_i^{\mathrm{L}} - \mu| \le r\sigma_0 \\ 0 & |\varepsilon_i^{\mathrm{L}} - \mu| > r\sigma_0 \end{cases} \quad (36)$$

where $\varepsilon_i^{\mathrm{L}}$ is the residual error of i_{th} term in (22), including $\varepsilon_{\mathrm{Y},i}^{\mathrm{L}}$ and $\varepsilon_{\mathrm{Z},i}^{\mathrm{L}}$, which are obtained with the left boundary of X into (22); μ is the mean of residual error; σ_0 is the standard deviation of residual error; s and r are the coefficients to assure robustness; s can be 1.0 $\sim$ 1.5, while r can be 2.5 $\sim$ 3.0. $s =$ 1.5 and $r =$ 3.0 are used in this paper.

If boundary conditions in (36) are obtained based on the mean and standard deviation of residuals directly, they will be affected by abnormal data and measurement error of different equipment. Thus, this paper applies the median estimator to calculate the distribution of residuals adaptively [40], i.e.,

$$\hat{\mu} \cong \mathrm{median}(\boldsymbol{\varepsilon}^{\mathrm{L}}) \quad (37)$$

$$\hat{\sigma}_0 \cong \frac{\mathrm{median}|\boldsymbol{\varepsilon}^{\mathrm{L}} - \hat{\mu}|}{0.6745} \quad (38)$$

where $\mathrm{median}(\boldsymbol{\varepsilon}^{\mathrm{L}})$ represents the median of the residual sequence $\boldsymbol{\varepsilon}^{\mathrm{L}} = [\boldsymbol{\varepsilon}_1^{\mathrm{L}}, \boldsymbol{\varepsilon}_2^{\mathrm{L}}, \cdots, \boldsymbol{\varepsilon}_n^{\mathrm{L}}]$. When the number of samples is large enough, mean and standard deviation can be estimated effectively by (37) and (38) without being affected by abnormal data. The median estimator has strong robustness.

The IGG robust method can also distinguish normal and abnormal data. Specifically, the weight of abnormal data is 0, while the weight of normal data is not 0. In the solution process, the objective function must keep unchanged, i.e., weight is the same in each iteration in linear approximation and accurate estimation. In this paper, the weights are determined based on the residual that is obtained by taking the left boundary of X into (22).

E. Flowchart for PAD Correction

The robust correction of PADs can be divided into 4 parts, i.e., weights determination based on IGG, linear estimation for PADs, rough identification for ParTL, and accurate estimation for PADs, and the overall process is shown in Fig. 7.

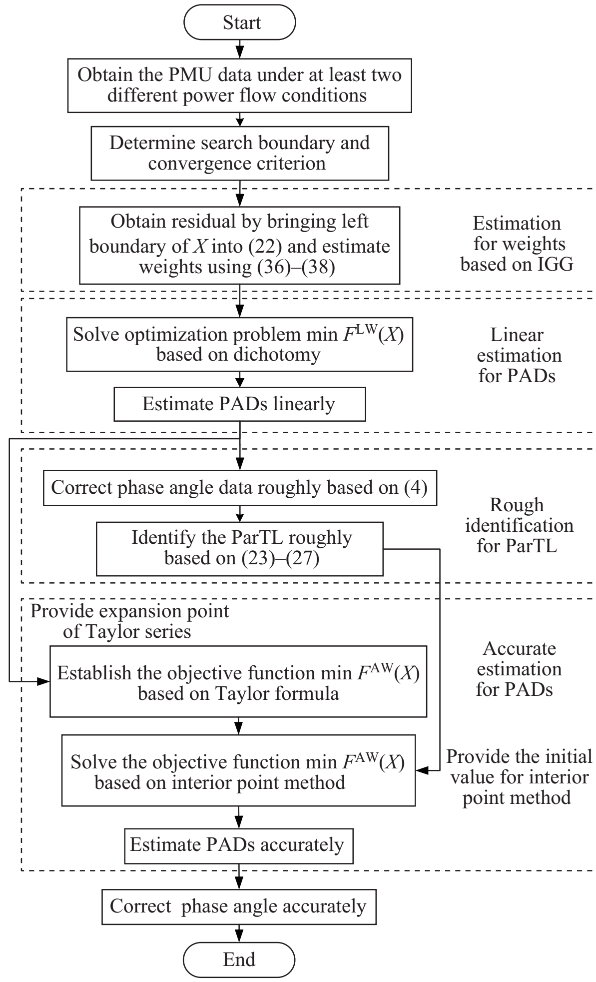

Fig. 7. Flowchart for PAD correction.

V. NUMERICAL RESULTS

In this section, the effectiveness of the proposed methods is verified with different noises and power flows. Besides, the robustness of the proposed methods is tested. Specifically, a 500 kV TL is modeled in PSCAD with parameters: length = 200 km, $R = 2.666\ \Omega$, $X = 40.448\ \Omega$, $Y = 7.6202 \times 10^{-4}$ S, and the upload period is 40 ms. Multiple sets of steady-state measurements are obtained by changing the load. Each set contains 1000 snapshot (40 s) measurements. Each simulation is conducted based on two sets of simulated measurements under different power flow conditions, and the loads and PADs of two power flows are denoted as P_{n1} and P_{n2}, $\theta_{V,Pn1}$ and $\theta_{V,Pn2}$. Besides, without repeating the description, the search boundary of dichotomy is set to be $[0.6X_{\mathrm{offline}}, 1.4X_{\mathrm{offline}}]$, and the left boundary is used to determine weight by default. In each case, 1000 Monte Carlo simulations are carried out and the average value is taken as the final result. All the simulated cases are performed on an Intel i5-10400 CPU, 16G RAM desktop.

A. Sensitivity to Noise

This case verifies the effectiveness of the proposed methods under different noises. Specifically, simulated data without noise under two power flow conditions are obtained by setting loads as 160+j16MVA and 180+j18MVA. Corresponding estimated results and their average relative error of linear approximation and accurate estimation based on F_{Y}-IGG and F_{Z}-IGG are shown in Table I.

As shown in Table I, when data do not contain noise, linear estimation results of the two models have a slightly larger error, but they are still near the set value. This shows that linear estimation can provide an effective Taylor expansion point for accurate estimation. Besides, errors of accurate estimation of two models are small, indicating the second-order Taylor series improves the accuracy of the methods. Besides, both methods have high computational efficiency. Specifically, F_{Y}-IGG only needs 0.29 s to calculate the PADs of 1000 sets of PMU data (40 s), which is faster than F_{Z}-IGG (1.06 s). Running times of both methods (0.29 s and 1.06 s) are less than data acquisition

TABLE I
RELATIVE ERROR OF ESTIMATED PADS IN LINEAR ESTIMATION AND ACCURATE ESTIMATION WITHOUT NOISE

Model		Running time (s)		$\theta_{V,Pn1}$ (°)	$\theta_{V,Pn2}$ (°)
			Set value	4.3237	4.8469
**F_Y-IGG	Linear estimation	0.24	Estimated value	4.2852	4.8127
			*Rel. error (%)	−0.8902	−0.7066
	Accurate estimation	0.29	Estimated value	4.3238	4.8470
			*Rel. error (%)	0.0025	0.0020
**F_Z-IGG	Linear estimation	0.95	Estimated value	4.3068	4.8370
			*Rel. error (%)	−0.3900	−0.2049
	Accurate estimation	1.06	Estimated value	4.3238	4.8470
			*Rel. error (%)	0.0023	0.0019

*Rel. error presents relative error.
**F_Y-IGG and F_Z-IGG presents the estimated model with IGG.

time (40 s). Thus, they can be used for online applications.

Furthermore, under the same power flows, the performance of the methods under different noises is tested, including 70 dB, 65 dB and 60 dB. Estimation results are shown in Table II. It can be found that under the same level of noise, the accuracy of the two methods is close. With noise level increasing, the errors of the estimation results increase gradually, but the maximum error is only 1.0060%, which is still near the set value, indicating the methods are effective under different levels of noise.

B. Sensitivity to Operating Conditions

This case verifies the effectiveness of the proposed methods under different power flow operating conditions. Specifically, simulated data with 70 dB noise is obtained under different power flow conditions, including constant load ratios ($P_{n1}/P_{n2} = 1.25$) and different load ratios (P_{n1}/P_{n2} from 2 to 12), and the corresponding estimated results are shown in Table III. It can be observed the relative errors of estimated PADs are all small. Among them, the maximum error is only 0.85%, indicating that the proposed methods can estimate the PADs accurately under different operating conditions.

TABLE II
RELATIVE ERROR OF ESTIMATED PADS WITH NOISE OF DIFFERENT LEVEL

Noise level	Model		$\theta_{V,Pn1}$ (°)	$\theta_{V,Pn2}$ (°)
		set value	4.3237	4.8469
70 dB	F_Y-IGG	Estimated value	4.3028	4.8285
		Rel. error (%)	−0.4823	−0.3792
	F_Z-IGG	Estimated value	4.3386	4.8637
		Rel. error (%)	0.3447	0.3455
65 dB	F_Y-IGG	Estimated value	4.3004	4.8257
		Rel. error (%)	−0.5374	−0.4388
	F_Z-IGG	Estimated value	4.2986	4.8191
		Rel. error (%)	−0.5809	−0.5733
60 dB	F_Y-IGG	Estimated value	4.2880	4.8121
		Rel. error (%)	−0.8240	−0.7176
	F_Z-IGG	Estimated value	4.3666	4.8957
		Rel. error (%)	0.9918	1.0060

C. Robustness to Abnormal Data

In this subsection, the robustness of the proposed methods under abnormal data is tested. Specifically, the simulated data for 40 s are obtained with the load of 160+j16MVA and 180+j18MVA, and 70 dB noise is added. Besides, data during 0–12 s at bus m are set to be 0 to simulate abnormal data (they can also be regarded as data loss). Estimated results and relative error during 12–40 s are shown in Table IV. When there are abnormal data, the PAD correction results of F_Y and F_Z have large errors, while the correction results of F_Y-IGG and F_Z-IGG still have high accuracy, which means the IGG method can accurately identify abnormal data and set their weights to 0 to exclude the interference of abnormal data.

D. Comparison with Other Methods

1) Correction of constant PAD deviations

To further illustrate the advantage of the proposed methods, comparisons with [28] are performed. Specifically, with the same TL in Section V-A, the loads are set to be 160 MW, 161 MW, 162 MW, 163 MW, 164 MW, 165 MW. 100 groups of data are obtained for each power flow. Constant deviations are added to the phase angle data at bus m to simulate PAD deviations in practice. Estimation results for the two methods are shown in Table V. When PAD deviation is small, the estimated results of [28] are accurate. But with increase of PAD deviation, the estimation results of [28] are deviating from set value. The reason is, in [28], field data with deviations are taken as expansion points to calculate the ordinary differential equation. Thus, when deviation is large, results will be inaccurate. By contrast, the proposed methods can obtain accurate results under different PAD deviations, which show the superiority of the proposed methods.

2) Correction of Time-varying PAD Deviations

In this section, by correcting the time-varying PAD deviation, performance of the proposed methods is compared with [29] and [14]. Specifically, this case applies the same data

TABLE III
THE RELATIVE ERROR OF ESTIMATED PADS OF THE PROPOSED METHODS UNDER DIFFERENT POWER FLOW CONDITIONS

	Constant load ratio (P_{n1}/P_{n2} is constant)						
Power flow conditions	P_{n1} (MW)	50	100	200	320	640	1280
	P_{n2} (MW)	40	80	160	400	800	1600
	P_{n1}/P_{n2}	1.25	1.25	1.25	1.25	1.25	1.25
Rel. error of PADs (%)	F_Y-IGG	−0.85	−0.59	−0.44	−0.15	−0.04	0.03
	F_Z-IGG	0.18	−0.75	0.27	−0.19	−0.10	0.01
	Different load ratios ($P_{n1}/P_{n2} = 2 \sim 12$)						
Power flow conditions	P_{n1} (MW)	80	160	240	320	400	480
	P_{n2} (MW)	40	40	40	40	40	40
	P_{n1}/P_{n2}	2	4	6	8	10	12
Rel. error of PADs (%)	F_Y-IGG	−0.56	0.28	0.13	0.24	−0.10	−0.43
	F_Z-IGG	0.49	0.15	−0.19	0.03	−0.12	−0.39

TABLE IV
THE ESTIMATED RESULTS OF PADS WITH PARTIAL DATA LOSS

Model		$\theta_{V,Pn1}$ (°)	$\theta_{V,Pn2}$ (°)
	Set value	4.3237	4.8469
$F_{\rm Y}$-IGG	Estimated value	4.3017	4.8275
	Rel. error (%)	−0.5077	−0.4017
$F_{\rm Y}$	Estimated value	13.6586	5.7080
	Rel. error (%)	181.8000	114.1052
$F_{\rm Z}$-IGG	Estimated value	4.2900	4.8093
	Rel. error (%)	−0.7782	−0.7764
$F_{\rm Z}$	Estimated value	2.4097	1.5562
	Rel. error (%)	−50.2848	−41.6267

TABLE V
THE ESTIMATED RESULTS OF [28] AND PROPOSED METHODS UNDER DIFFERENT PAD DEVIATIONS

Set values of PAD deviation	Estimated results for PAD deviation		
	$F_{\rm Z}$-IGG	$F_{\rm Y}$-IGG	[28]
2	2.04	2.03	2.01
10	10.03	10.02	9.99
20	20.04	20.03	20.39
40	40.03	40.05	61.15

in Section V-A, and ramp time-varying phase angle deviation with a maximum value of 0.2° is added to the voltage and current phase angle data at bus m, as the black line shown in Fig. 8. Corrected results based on [14], [29], and the proposed methods are shown in Fig. 8, also. It can be found the corrected results of [14], [29] deviate from the set value. The reason is the methods in [29] and [14] assume the PAD deviation is constant during measurement period or a small period, which is not suitable for correction of time-varying deviation. By contrast, the corrected results of the proposed methods are close to the set value. This case demonstrates the effectiveness of the proposed methods in correcting time-varying PAD deviation.

VI. RESULTS WITH FIELD PMU DATA

This section applies the proposed methods to the actual data obtained from a 90.3 km long, 500 kV TL (mentioned in Section II). Specifically, PMU measurements (with a sampling

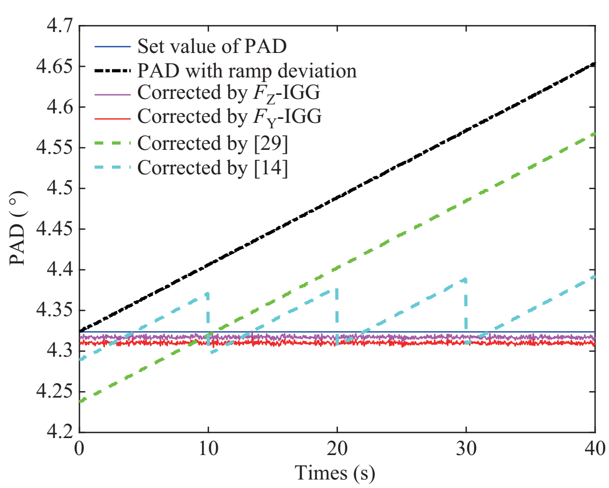

Fig. 8. The estimated results of [14], [29] and the proposed methods under time-varying PAD deviation.

period of 40 ms) under two different power flow conditions are used. Each condition contains 1,000 sets of PMU measurements. The correction results and field data under one working condition are shown in the Fig. 9.

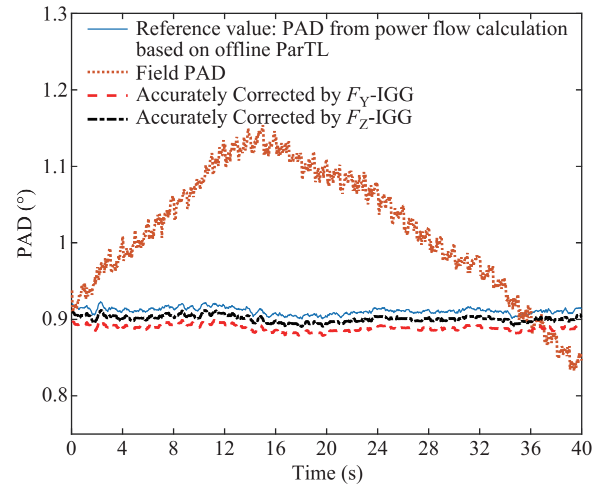

Fig. 9. Field PAD data, reference value of PAD, and corrected PAD data by the proposed methods with time-varying PAD deviations.

In Fig. 9, the orange dashed line is the field PMU data with time varying deviation; the red and black dashed line is the corrected results based on $F_{\rm Y}$-IGG and $F_{\rm Z}$-IGG, respectively; note, since the actual value of the PADs in practice is unknown, the PADs from power flow calculations based on offline ParTL are taken as the reference value instead of actual value, see the blue solid line.

It can be found the PADs estimated by the two methods are close, indicating they yield consistent results. Besides, compared with the field PADs before correction, the correction results by the proposed methods are far closer to the reference value, which shows the practicability of the proposed methods in correcting the time-varying PMU phase angle deviation.

Furthermore, with (23)–(24) and the corrected and uncorrected phase angle data under power flow 1, the ParTL can be identified at each snapshot. Taking the reactance as an example, the maximum, minimum, and median of identification results are shown in Table VI. It is observed the difference between the maximum and minimum values of the identified reactance based on the uncorrected data during 40 s are large, and the maximum value deviates from the offline value a lot. Identified reactance based on the corrected data fluctuates little and is close to the offline value.

TABLE VI
IDENTIFICATION RESULTS OF REACTANCE WITH CORRECTED AND UNCORRECTED PHASE ANGLE DATA

Statistical value	Uncorrected	$F_{\rm Y}$-IGG	$F_{\rm Z}$-IGG	Offline value
Maximum (Ω)	30.1013	24.0636	24.3419	
Minimum (Ω)	22.6812	23.8845	24.1620	23.8416
Median (Ω)	27.0678	23.9663	24.2441	

VII. CONCLUSION

This paper proposes two robust correction methods for time-varying PAD deviation without knowing ParTL. The methods are applicable to the case that the PMU are installed at both ends of the line, which is independent of the topology of power system. Correction is realized by converting the problem of estimating PADs to the estimation of the ParTL via linear approximation and accurate expression. Besides, by applying the "three-segment" IGG weight function to the PAD estimation, the proposed methods have the robustness to bypass abnormal data. If the phase angle errors caused by CT and PT are the same, the methods will combine the two types of errors automatically. Results with simulated and field data under different power flow conditions verify the effectiveness and robustness of the proposed methods.

REFERENCES

[1] Y. Liu, L. W. Zhan, Y. Zhang, P. N. Markham, D. Zhou, J. H. Guo, Y. Lei, G. F. Kou, W. X. Yao, J. D. Chai, and Y. L. Liu, "Wide-area-measurement system development at the distribution level: An FNET/GridEye example," *IEEE Transactions on Power Delivery*, vol. 31, no. 2, pp. 721–731, Apr. 2016.

[2] A. G. Phadke and T. S. Bi, "Phasor measurement units, WAMS, and their applications in protection and control of power systems," *Journal of Modern Power Systems and Clean Energy*, vol. 6, no. 4, pp. 619–629, Jul. 2018.

[3] L. Xie, Y. Chen, and P. R. Kumar, "Dimensionality reduction of synchrophasor data for early event detection: Linearized analysis," *IEEE Transactions on Power Systems*, vol. 29, no. 6, pp. 2784–2794, Nov. 2014.

[4] C. Wang, Z. J. Qin, Y. H. Hou, and J. Yan, "Multi-area dynamic state estimation with PMU measurements by an equality constrained extended Kalman filter," *IEEE Transactions on Smart Grid*, vol. 9, no. 2, pp. 900–910, Mar. 2018.

[5] J. B. Zhao, G. X. Zhang, K. Das, G. N. Korres, N. M. Manousakis, A. K. Sinha, and Z. Y. He, "Power system real-time monitoring by using PMU-based robust state estimation method," *IEEE Transactions on Smart Grid*, vol. 7, no. 1, pp. 300–309, Jan. 2016.

[6] J. Sun, Q. Chen and M. Xia, "Data-driven detection and identification of line parameters with PMU and unsynchronized SCADA measurements in distribution grids," *CSEE Journal of Power and Energy Systems*, doi: 10.17775/CSEEJPES.2020.06860.

[7] W. X. Yao, Y. Liu, D. Zhou, Z. H. Pan, M. J. Till, J. C. Zhao, L. Zhu, L. W. Zhan, Q. Tang, and Y. L. Liu, "Impact of GPS signal loss and its mitigation in power system synchronized measurement devices," *IEEE Transactions on Smart Grid*, vol. 9, no. 2, pp. 1141–1149, Mar. 2018.

[8] A. C. Xue, F. Y. Xu, J. H. Chow, S. Leng, H. Kong, J. S. Xu, and T. S. Bi, "Data-driven detection for GPS spoofing attack using phasor measurements in smart grid," *International Journal of Electrical Power & Energy Systems*, vol. 129, pp. 106883, Jul. 2021.

[9] E. Shereen and G. Dán, "Model-based and data-driven detectors for time synchronization attacks against PMUs," *IEEE Journal on Selected Areas in Communications*, vol. 38, no. 1, pp. 169–179, Jan. 2020.

[10] S. Pal, B. Sikdar, and J. H. Chow, "Classification and detection of PMU data manipulation attacks using transmission line parameters," *IEEE Transactions on Smart Grid*, vol. 9, no. 5, pp. 5057–5066, Sep. 2018.

[11] W. P. Yu, W. X. Yao, X. D. Deng, Y. F. Zhao, and Y. L. Liu, "Timestamp shift detection for synchrophasor data based on similarity analysis between relative phase angle and frequency," *IEEE Transactions on Power Delivery*, vol. 35, no. 3, pp. 1588–1591, Jun. 2020.

[12] W. X. Yao, Z. S. Teng, Q. Tang, and Y. P. Gao, "Power system phasor measurement and correction algorithm under asynchronous sampling," *Chinese Journal of Scientific Instrument*, vol. 34, no. 7, pp. 1518–1524, (2013).

[13] T. S. Bi, J. R. Guo, K. Xu, L. Zhang, and Q. X. Yang, "The impact of time synchronization deviation on the performance of synchrophasor measurements and wide area damping control," *IEEE Transactions on Smart Grid*, vol. 8, no. 4, pp. 1545–1552, Jul. 2017.

[14] A. C. Xue, F. Y. Xu, J. S. Xu, J. H. Chow, S. Leng, and T. S. Bi, "Online pattern recognition and data correction of PMU data under GPS spoofing attack," *Journal of Modern Power Systems and Clean Energy*, vol. 8, no. 6, pp. 1240–1249, Nov. 2020.

[15] B. Trinchera, D. Serazio, and U. Pogliano, "Asynchronous phase comparator for characterization of devices for PMUs calibrator," *IEEE Transactions on Instrumentation and Measurement*, vol. 66, no. 6, pp. 1139–1145, Jun. 2017.

[16] J. Li, S. Xu, H. Liu and T. Bi, "High-accuracy and low-complexity phasor estimation method for PMU calibration," *CSEE Journal of Power and Energy Systems*, vol. 7, no. 6, pp. 1202–1212, Nov. 2021, doi: 10.17775/CSEEJPES.2020.01180.

[17] L. W. Zhan, Y. Liu, and Y. L. Liu, "A Clarke transformation-based DFT phasor and frequency algorithm for wide frequency range," *IEEE Transactions on Smart Grid*, vol. 9, no. 1, pp. 67–77, Jan. 2018.

[18] P. Zhang, H. Xue, R. G. Yang, and J. Zhang, "Shifting window average method for phasor measurement at offnominal frequencies," *IEEE Transactions on Power Delivery*, vol. 29, no. 3, pp. 1063–1073, Jun. 2014.

[19] D. Macii, D. Petri, and A. Zorat, "Accuracy analysis and enhancement of DFT-based synchrophasor estimators in off-nominal conditions," *IEEE Transactions on Instrumentation and Measurement*, vol. 61, no. 10, pp. 2653–2664, Oct. 2012.

[20] T. Jin and W. F. Zhang, "A novel interpolated DFT synchrophasor estimation algorithm with an optimized combined cosine self-convolution window," *IEEE Transactions on Instrumentation and Measurement*, vol. 70, pp. 9000610, 2021.

[21] X. Y. Fan, L. Du, and D. L. Duan, "Synchrophasor data correction under GPS spoofing attack: A state estimation-based approach," *IEEE Transactions on Smart Grid*, vol. 9, no. 5, pp. 4538–4546, Sep. 2018.

[22] L. Vanfretti, J. H. Chow, S. Sarawgi, and B. Fardanesh, "A phasor-data-based state estimator incorporating phase bias correction," *IEEE Transactions on Power Systems*, vol. 26, no. 1, pp. 111–119, Feb. 2011.

[23] Y. Zhang, J. H. Wang, and J. Z. Liu, "Attack identification and correction for PMU GPS spoofing in unbalanced distribution systems," *IEEE Transactions on Smart Grid*, vol. 11, no. 1, pp. 762–773, Jan. 2020.

[24] P. Risbud, N. Gatsis, and A. Taha, "Multi-period power system state estimation with PMUs under GPS spoofing attacks," *Journal of Modern Power Systems and Clean Energy*, vol. 8, no. 4, pp. 597–606, Jul. 2020.

[25] Q. Dong, C. Ma, and F. Han, "Method for calculating phase angle difference between voltage phasors using phase angle data measured with DFT," *Power System Technology*, vol. 41, no. 9, pp. 2996–3002, Sep. 2017.

[26] D. Shi, D. J. Tylavsky, and N. Logic, "An adaptive method for detection and correction of errors in PMU measurements," *IEEE Transactions on Smart Grid*, vol. 3, no. 4, pp. 1575–1583, Dec. 2012.

[27] Q. Zhang, V. Vittal, G. T. Heydt, N. Logic, and S. Sturgill, "The integrated calibration of synchronized phasor measurement data in power transmission systems," *IEEE Transactions on Power Delivery*, vol. 26, no. 4, pp. 2573–2581, Oct. 2011.

[28] X. Wang, D. Shi, Z. W. Wang, C. L. Xu, Q. B. Zhang, X. H. Zhang, and Z. Yu, "Online calibration of phasor measurement unit using density-based spatial clustering," *IEEE Transactions on Power Delivery*, vol. 33, no. 3, pp. 1081–1090, Jun. 2018.

[29] A. C. Xue, F. Y. Xu, J. S. Xu, J. H. Chow, H. Y. You, and T. S. Bi, "Correction of phasor measurements independent of transmission line parameters," *IEEE Transactions on Smart Grid*, vol. 11, no. 1, pp. 346–356, Jan. 2020.

[30] A. Pal, P. Chatterjee, J. S. Thorp, and V. A. Centeno, "Online calibration of voltage transformers using synchrophasor measurements," *IEEE Transactions on Power Delivery*, vol. 31, no. 1, pp. 370–380, Feb. 2016.

[31] J. B. Zhao, S. Fliscounakis, P. Panciatici, and L. Mili, "Robust parameter estimation of the French power system using field data," *IEEE Transactions on Smart Grid*, vol. 10, no. 5, pp. 5334–5344, Sep. 2019.

[32] D. L. Duan, L. Q. Yang, and L. L. Scharf, "Phasor state estimation from PMU measurements with bad data," in *Proceedings of the 4th IEEE International Workshop on Computational Advances in Multi-Sensor Adaptive Processing (CAMSAP)*, San Juan, USA, 2011, pp. 121–124.

[33] Y. Z. Lin and A. Abur, "A highly efficient bad data identification approach for very large scale power systems," *IEEE Transactions on Power Systems*, vol. 33, no. 6, pp. 5979–5989, Nov. 2018.

[34] M. Wu and L. Xie, "Online detection of low-quality synchrophasor measurements: A data-driven approach," *IEEE Transactions on Power Systems*, vol. 32, no. 4, pp. 2817–2827, Jul. 2017.

[35] A. C. Xue, F. Y. Xu, K. E. Martin, J. S. Xu, H. Y. You, and T. S. Bi, "Linear approximations for the influence of phasor angle difference errors on line parameter calculation," *IEEE Transactions on Power Systems*, vol. 34, no. 5, pp. 3455–3464, Sep. 2019.

[36] H. Y. You, "Transmission line parameter identification based on PMU and SCADA data," M.S. thesis, Department, North China Electric Power University (Beijing), Beijing, 2018.

[37] V. Cecchi, K. Miu, A. S. Leger, and C. Nwankpa, "Study of the impacts of ambient temperature variations along a transmission line using temperature-dependent line models," in *Proceedings of 2011 IEEE Power and Energy Society General Meeting*, 2011, pp. 1–7, doi: 10.1109/PES.2011.6039110.

[38] A. C. Xue, F. Y. Xu, K. E. Martin, H. Y. You, J. S. Xu, L. Wang, and G. E. Wei, "Robust identification method for transmission line parameters that considers PMU phase angle error," *IEEE Access*, vol. 8, pp. 86962–86971, May. 2020.

[39] J. Zhou, Development of robust estimation theory. Robust Least Squares, Wuhan, China: Huazhong University of Science and Technology Press,, 1997, pp. 7–10

[40] A. C. Xue, Z. Y. Zhang, and T. S. Bi, "Online identification of transmission line positive-sequence parameters based on adaptive robust least squares," *Transactions of China Electrotechnical Society*, vol. 30, no. 8, pp. 202–209, Apr. 2015.

Ancheng Xue (M'08) received a B.Sc. degree in Applied Mathematics and a Ph.D. degree in Electrical Engineering both from Tsinghua University, Beijing, China, in 2001 and 2006, respectively. He was a post-doctor at the Institute of System Science, Chinese Academy of Sciences. Currently, he is a Professor with the School of Electrical and Electronic Engineering, North China Electric Power University, where he joined in March 2008. His research interests include data-driven power system analysis, control and protection.

He Kong (S'20) is currently pursuing his Ph.D. degree at North China Electric Power University. At the same university, he got his B.S degree in Electrical Engineering. His research interests include the application of PMU in power systems and the transient voltage stability.

Feiyang Xu (S'18) is pursuing his Ph.D. degree at North China Electric Power University where he obtained a B.Sc. degree in Electrical Engineering. His research interest is application of PMU in power systems.

Junbo Zhao is an Assistant Professor of the Department of Electrical and Computer Engineering at the University of Connecticut. He was an Assistant Professor and research assistant professor at Mississippi State University and Virginia Tech from 2019–2021 and 2018–2019, respectively. He received a Ph.D. degree from Bradley Department of Electrical and Computer Engineering Virginia Tech, in 2018. He was a Research Assistant Professor at Virginia Tech from May 2018 to August 2019. He did a summer internship at Pacific Northwest National Laboratory from May to August 2017. He is currently the chair of the IEEE Task Force on Power System Dynamic State and Parameter Estimation, the IEEE Task Force on Cyber-Physical Interdependency for Power System Operation and Control, co-chair of the IEEE Working Group on Power System Static and Dynamic State Estimation, the Secretary of the IEEE PES Bulk Power System Operation Subcommittee and officer of the IEEE PES Renewable Systems Integration Coordinating Committee.

Naichao Chang received a B.E. and Ph.D. degrees in Electrical Engineering from the Harbin Institute of Technology, Harbin, China in 1999 and 2004, respectively. He was a Postdoctoral Research Fellow with the University of Hong Kong, Hong Kong, China, from 2004 to 2006, and a Postdoctoral Research Fellow with Tsinghua University, Beijing, China, from 2006 to 2008. He joined the National Electric Power Dispatching and Control Center, State Grid Corporation of China, Beijing, China, in 2008, where he is currently a professorate senior engineer of the Automation Department. His research interests include advanced applications of EMS and renewable energy integration of power systems.

Joe H. Chow received M.S. and Ph.D. degrees from the University of Illinois, Urbana-Champaign, USA. After working in the General Electric power system business in Schenectady, NY, USA, he joined Rensselaer Polytechnic Institute, Troy, NY, USA, in 1987, where he is an Institute Professor of Electrical, Computer, and Systems Engineering. He is a Life Fellow of IEEE, a Member of the US National Academy of Engineering, and a Foreign Fellow of CSEE.

Haiyan Hong is pursuing her master degree at North China Electric Power University where she obtained a B.Sc. degree in Electrical Engineering. Her research interest is the application of PMU in power systems.